Available online at www.sciencedirect.com
ScienceDirect
Journal of Sound and Vibration 305 (2007) 272–288
JOURNAL OF SOUND AND VIBRATION
www.elsevier.com/locate/jsvi

Acoustically coupled model of an enclosure and a Helmholtz resonator array

Deyu Li, Li Cheng*

Department of Mechanical Engineering, The Hong Kong Polytechnic University, Hung Home, Kowloon, Hong Kong, SAR, China

Received 29 June 2006; received in revised form 20 March 2007; accepted 5 April 2007
Available online 22 May 2007

Abstract

This paper presents a general model for dealing with acoustic coupling between an enclosure and a Helmholtz resonator array, which leads to a special model when the array retreats to one resonator. The general model considers a significant number of enclosure modes, resonators, and sources, and gives more accurate prediction results without suffering from the singularity problem met before. The development of the special model results in a rigorous analytical solutions, which allows us to reexamine some of the previous studies reported in literatures. Based on the special model, a frequency equation to predict the frequency variation at both the targeted and off-target modes due to inserting a resonator into the enclosure is provided, and a method to constrain the worsened noise level at off-target modes is also discussed. Comparisons are made among computed data using the present model, previously published models, and measured results, and generally favorable agreement between prediction and measurement is observed. The present model is helpful to numerically evaluate the noise control performance of a resonator array installed in an enclosure, and also useful to semi-analytically determine the optimal location for resonators, which currently still involves heavy experimental measurements on a trial-and-error basis.
© 2007 Elsevier Ltd. All rights reserved.

1. Introduction

Helmholtz resonators are often used as a narrowband sound absorption device in the noise control of a reverberant enclosure. When a well designed and tuned resonator is put in the enclosure at a location not too near the node of targeted mode, the force produced by the incident sound pressure over the aperture of the resonator drives the lumped air-mass inside the resonator neck to vibrate. Due to the natural frequency matching between the resonator and the targeted enclosure mode, the resonance occurs in the resonator, such trapping most of the input energy in a relative narrowband between two coupled frequencies [1]. The volume velocity out of the resonator aperture forms an effective secondary source inside the enclosure. The results of acoustic interaction between the primary and secondary sound field in the enclosure and the energy dissipated in the resonator itself provide attenuation of the unwanted sound in the enclosure.

*Corresponding author. Tel.: +852 2766 6769; fax: +852 2365 4703.
E-mail address: mmlcheng@polyu.edu.hk (L. Cheng).

0022-460X/$ - see front matter © 2007 Elsevier Ltd. All rights reserved.
doi:10.1016/j.jsv.2007.04.009

Several authors have investigated the acoustic interaction when introducing Helmholtz resonators into rooms [1–4]. Van Leeuwen [2] examined the coupling between a room mode and a Helmholtz resonator using electrical analog method. Fahy and Schofield [1] conducted theoretical and experimental research to improve the work in Ref. [2]. In Ref. [1], it was assumed that the average separation between resonance frequencies of the room was sufficiently large to exceed the average modal bandwidth. In that sense, only the targeted particular room mode (single-mode) was taken into account in the coupling analysis and all other room modes were negligible due to their remoteness in frequency from that of the resonator. Based on this assumption, formulas and charts were presented, which were very helpful to understand the absorptive mechanism of the resonator and to optimally design a single Helmholtz resonator. However, in most of cases, acoustic modes of a room may not be well separated in frequency due to a relatively high modal-density. Moreover, a resonator array consisting of multiple resonators may be required in some practical applications to control one or several different room modes simultaneously. Therefore, an acoustic coupling model considering the interaction between multiple enclosure modes and multiple resonators is desired. In this regard, Cummings [4] presented a multimode theory to replace the single-mode treatment for the interaction between an array of resonators and the sound field generated by an arbitrary source distribution in the room. In his work, the resonator was assumed to behave like a point source. The volume velocity of each acoustic resonator was solved from a series of linear equations obtained from balancing pressures at each resonator aperture. Cummings pointed out that since the resonator was taken as a continuous point source, the sound pressure at the resonator aperture was singular if the pressure was calculated from its own volume velocity. Thus, he used an average sound pressure at the surface of a small equivalent pulsating sphere to replace the singular sound pressure directly radiated from the point source of the resonator at its own location [4]. It is found out in the present paper that the coupled frequencies obtained from the equivalent sphere model led to a relatively large discrepancy with the measurement.

In the present study, a multimode theory for describing the acoustic interaction between an enclosure and a Helmholtz resonator array is developed. It is a direct expansion of Fahy and Scholfield's work to the case of multiple room modes coupled with multiple acoustic resonators and multiple sound sources. This model does not suffer from the "pitfall" of the singularity problem encountered in Ref. [4]. As a special case, the coupling problem between one enclosure and only one resonator is further investigated to reveal the underlying physics in complex mathematical equations in the general model. Analytical solutions of the pressure field in the enclosure and the volume velocity source strength out of the resonator are derived without any extra hypotheses but just by means of mathematical manipulation. Comparisons among predictions based on the current theory and Cummings's theory [4] as well as the measured data presented by Fahy and Schofield [1] have been carried out, and certain features peculiar to the present models have been examined.

2. Theory

A general model comprising an enclosure coupled with an acoustic resonator array is presented before investigating a special case of the enclosure coupled with only one resonator. Both classical Helmholtz resonators and quarter wavelength resonators can be used. For a classical Helmholtz resonator, its effective neck length includes both exterior [5] and interior [6] end corrections to consider the local reactive effects [1] and to release the pressure in the aperture [7]. However, the resistance of the resonator only accounts for the interior resistance in its neck whilst excluding the external radiation resistance because it has been taken into account in the enclosure sound field [1]. For a quarter wavelength resonator without porous material installed in the tube, the effective length only includes the exterior end correction.

2.1. General coupling model of an enclosure with an acoustic resonator array

It is assumed that M acoustic resonators are located at the points $\mathbf{r}_1^R, \mathbf{r}_2^R, \ldots, \mathbf{r}_M^R$ (centers of the resonator apertures) in an enclosure, in which a set of N harmonic point sources with volume velocity source strength density $q_1^S, q_2^S, \ldots, q_N^S$, centered at the points $\mathbf{r}_1^R, \mathbf{r}_2^R, \ldots, \mathbf{r}_N^R$ are arbitrarily distributed. Here, the superscripts R and S indicate the variables associated with "Resonator" and "Source", respectively. For the resonator m in the array, the air inside its neck is simplified as a lumped mass and its motion follows the Newton's second law

provided that the geometric dimensions of the resonator aperture is very small compared with the targeted sound wavelength:

$$\rho_0 L_m^R S_m^R \ddot{x}_m^R(t) + S_m^R R_{im} \dot{x}_m^R(t) + \frac{\rho_0 c^2 \left(S_m^R\right)^2}{V_m^R} x_m^R(t) = -p(\mathbf{r}_m^R, t) S_m^R, \tag{1}$$

where $x(t)$ is the particle displacement, which is assumed positive when it points to the enclosure, S_m^R the cross sectional area of the aperture, V_m^R the volume of the resonator body, L_m^R the effective length, R_{im} the internal resistance of the resonator neck, and $p(\mathbf{r}_m^R, t)$ the average sound pressure over the aperture area. Eq. (1) can be simplified as

$$\ddot{x}_m^R(t) + cR_m \dot{x}_m^R(t) + \left(\omega_m^R\right)^2 x_m^R(t) = -\frac{1}{\rho_0 L_m^R} p(\mathbf{r}_m^R, t), \tag{2}$$

where $\left(\omega_m^R\right)^2 = c^2 S_m^R / L_m^R V_m^R$, ω_m^R is the radian natural frequency of the resonator m, $R_m = R_{im}/z_0 L_m^R$ and $z_0 = c\rho_0$, z_0 the characteristic impedance of the air.

Each vibrating resonator creates an effective sound source (secondary sound source) with a volume velocity source strength density $q_m^R(t) = S_m^R \dot{x}_m^R(t)\delta(\mathbf{r} - \mathbf{r}_m^R)$ directed out of the resonator aperture into the enclosure [1]. Therefore, the sound field in the enclosure is the superposition of the primary and the secondary sound fields. Thus, an inhomogeneous wave equation which governs the behavior of the air in the enclosure is

$$\nabla^2 \phi(\mathbf{r}, t) - \frac{1}{c^2} \ddot{\phi}(\mathbf{r}, t) = \sum_{m=1}^{M} S_m^R \dot{x}_m^R(t) \delta(\mathbf{r} - \mathbf{r}_m^R) + \sum_{n=1}^{N} q_n^S(t) \delta(\mathbf{r} - \mathbf{r}_n^S), \tag{3}$$

where $\phi(\mathbf{r}, t)$ is the acoustic velocity potential, $\delta(\mathbf{r}-\mathbf{r}_0)$ the three dimensional Dirac delta function. $\phi(\mathbf{r}, t)$ can be expanded on the basis of eigenfunctions of the enclosure $\phi(\mathbf{r}, t) = \sum_j^J \psi_j(t)\varphi_j(\mathbf{r})$, where J is the maximum mode number of the enclosure under consideration, $\psi_j(t)$ is the jth modal response, and $\varphi_j(\mathbf{r})$ is the jth eigenfunction. Applying orthogonality properties of the acoustic modes to the wave Eq. (3) yields a discretized equation

$$\ddot{\psi}_j(t) + \left(\gamma_j^E\right)^2 \psi_j(t) = -\frac{c^2}{V^E} \sum_{m=1}^{M} \frac{\varphi_j(\mathbf{r}_m^R)}{\Lambda_j^E} S_m^R \dot{x}_m^R(t) - \frac{c^2}{V^E} \sum_{n=1}^{N} \frac{\tilde{\varphi}_j(\mathbf{r}_n^S)}{\Lambda_j^E} q_n^S(t), \tag{4}$$

where V^E is the volume of enclosure, Λ_j^E the mode normalization factor, given by $\Lambda_j^E = \int_{V^E} [\varphi_j(\mathbf{r})]^2 \, \mathrm{d}V / V^E$, $\tilde{\varphi}_j(\mathbf{r}_n^S)$ the average of $\varphi_j(\mathbf{r}_n^S)$ over the volume of the nth source, and γ_j^E the jth complex eigenvalue of the enclosure, expressed as $\gamma_j^E = \omega_j^E + \mathrm{i}C_j^E$, in which the real part is the radian natural frequency and the imaginary part is an equivalent *ad hoc* damping coefficient.

Using $p(\mathbf{r}_m^R, t) = -\rho_0 \dot{\phi}(\mathbf{r}, t)\delta(\mathbf{r} - \mathbf{r}_m^R)$ and $\phi(\mathbf{r}, t) = \sum \psi_j(t)\varphi_j(\mathbf{r})$, Eq. (2) can be expressed as

$$\ddot{x}_m^R(t) + cR_m \dot{x}_m^R(t) + \left(\omega_m^R\right)^2 x_m^R(t) = \frac{1}{L_m^R} \sum_{h=1}^{J} \dot{\psi}_h(t) \varphi_h(\mathbf{r}_m^R). \tag{5}$$

Assuming the time harmonic variables are $\psi_j(t) = P_j \mathrm{e}^{\mathrm{i}\omega t}$, $x_m^R(t) = X_m^R \mathrm{e}^{\mathrm{i}\omega t}$, and $q_n^S(t) = Q_n^S \mathrm{e}^{\mathrm{i}\omega t}$, Eqs. (4) and (5) become, respectively,

$$\left[\omega^2 - \left(\gamma_j^E\right)^2\right] P_j = \frac{c^2}{V^E} \sum_{m=1}^{M} \frac{\mathrm{i}\omega S_m \varphi_j(\mathbf{r}_m^R)}{\Lambda_j} X_m^R + \frac{c^2}{V^E} \sum_{n=1}^{N} \frac{\tilde{\varphi}_j(\mathbf{r}_n^S)}{\Lambda_j} Q_n^S \tag{6}$$

and

$$\left[\left(\omega_m^R\right)^2 - \omega^2 + \mathrm{i}cR_m\omega\right] X_m^R = \frac{\mathrm{i}\omega}{L_m^R} \sum_{h=1}^{J} \varphi_h(\mathbf{r}_m^R) P_h. \tag{7}$$

Solving Eq. (7) yields

$$X_m^R = \frac{\mathrm{i}\omega}{\left[\left(\omega_m^R\right)^2 - \omega^2 + \mathrm{i}cR_m\omega\right]} \frac{1}{L_m^R} \sum_{h=1}^{J} \varphi_h(\mathbf{r}_m^R) P_h. \tag{8}$$

Substituting Eq. (8) into Eq. (6) gives

$$\left\{ \frac{\omega^2 - \left(\lambda_j^E\right)^2}{\omega^2} - \sum_{m=1}^{M} A_m^R \frac{V_m^R}{V^E} \frac{\left[\varphi_j(\mathbf{r}_m^R)\right]^2}{\Lambda_j} \right\} \frac{P_j}{\dfrac{Q^S}{k^2 V^E}},$$
$$- \sum_{h \neq j}^{J} \left[\sum_{m=1}^{M} A_m^R \frac{V_m^R}{V^E} \frac{\varphi_j(\mathbf{r}_m^R)\varphi_h(\mathbf{r}_m^R)}{\Lambda_j} \right] \frac{P_h}{\dfrac{Q^S}{k^2 V^E}} = \sum_{n=1}^{N} \frac{\tilde{\varphi}_j(\mathbf{r}_n^S)}{\Lambda_j} \frac{Q_n^S}{Q^S}, \tag{9}$$

where

$$A_m^R = \frac{\left(\omega_m^R\right)^2}{\omega^2 - \mathrm{i}cR_m\omega - \left(\omega_m^R\right)^2}, \tag{10}$$

where A_m^R is defined as the acoustic parameter of the mth Helmholtz resonator, and Q^S the volume velocity source strength of one primary point source. Eq. (9) is a set of linear equations when only J enclosure modes are considered. The modal response P_j can be numerically solved when the eigenvalues and eigenfunctions of the enclosure are known and the installed resonators and the distributed primary point sources are also given. The sound pressure $p(\mathbf{r})$ can be computed from $p(\mathbf{r}) = -\rho_0 \dot{\phi}(\mathbf{r})$:

$$\frac{p(\mathbf{r})}{\dfrac{\mathrm{i}\omega\rho_0 Q^S}{k^2 V^E}} = -\sum_{j=1}^{J} \left[\varphi_j(\mathbf{r}) \left(\frac{P_j}{\dfrac{Q^S}{V^E k^2}} \right) \right]. \tag{11}$$

In the absence of the resonators, i.e., $A_m^R = 0$, the modal response P_j can be analytically solved from Eq. (9) as

$$\frac{P_j}{\dfrac{Q^S}{k^2 V^E}} = \frac{\omega^2}{\omega^2 - \left(\gamma_j^E\right)^2} \sum_{n=1}^{N} \left[\frac{\tilde{\varphi}_j(\mathbf{r}_n^S)}{\Lambda_j} \frac{Q_n^S}{Q^S} \right] \quad (j = 1, 2, 3, \ldots, J). \tag{12}$$

As an example, a special case involving identical resonators to target the enclosure mode H is examined. Assuming that the average separation of the natural frequencies of the enclosure mode greatly exceeds the average modal bandwidth, only mode H is kept in the acoustic coupling. Expressing $\omega_m^R = \omega^R$, $V_m^R = V^R$, $L_m^R = L^R$ and $R_m = R$, the modal response P_H can be approximately obtained from Eq. (9) as

$$\frac{P_H}{\dfrac{Q^S}{k^2 V^E}} = \frac{\displaystyle\sum_{n=1}^{N} \frac{\tilde{\varphi}_H(\mathbf{r}_n^S)}{\Lambda_H} \frac{Q_n^S}{Q^S}}{\dfrac{\omega^2 - \left(\gamma_H^E\right)^2}{\omega^2} - \underbrace{A^R \frac{V^R}{V^E} \sum_{m=1}^{M} \frac{\varphi_H^2(\mathbf{r}_m^R)}{\Lambda_H}}_{\text{contribution from resonators}}}. \tag{13}$$

Comparing Eq. (12) with Eq. (13) it can be seen that the effect of the resonators is reflected by an additional term appearing in the denominator in Eq. (13). At the targeted enclosure natural frequency (i.e., $\omega = \omega_H = \omega^R$), the term $[\omega^2 - (\gamma_H^E)^2/\omega^2]$ vanishes due to the lightly damped enclosure. By the same token, the term $A^R V^R \sum_{m=1}^{M} [\varphi_H^2(\mathbf{r}_m^R)]/V^E \Lambda_H$ dominates, controlling the behavior of the enclosure at the targeted

resonance. More specifically, the term $\sum_{m=1}^{M} \varphi_H^2(\mathbf{r}_m^R)/\Lambda_H$, which is location dependent, conveys two important messages: (1) The most effective control occurs when the resonator apertures are located in anti-nodes of the targeted enclosure mode where the strongest coupling happens; (2) increasing the number of the resonators can improve modal response of P_H around the targeted resonance frequency provided the center distance of any two resonators is larger than a quarter wavelength of interesting sound leading to a negligible interaction among the resonator themselves [8,9].

2.2. Acoustic coupling model of an enclosure with only one acoustic resonator

It has been reported that when introducing a resonator or a resonator array into an enclosure, the targeted mode can be well controlled but other off-target modes may either be improved or deteriorated [10]. This phenomenon cannot be analytically explained using Fahy and Schofield's model [1] because only the targeted mode was considered in their solution. From Cummings's general model, one can obtain a solution for the volume velocity source strength of the resonator and then solve the sound pressure inside the enclosure. However, in order to solve the singularity problem in Cumming's model, an equivalent sphere was used to approximate the resonator radiation, which resulted in a relatively large discrepancy in the prediction of coupled frequencies when comparing with experimental results as we will show later. Any coupled system, such as the present one with multiple resonators, behaves like the general structural and acoustic interaction model presented by Dowell et al. [11] and Fahy [12]. The discretized modal equations generally involve integral operations over the interface surface between the structure and acoustic system. In that case, no analytical solution can be obtained without further hypotheses and simplifications. However, the coupling between a single-degree-of-freedom (sdof) Helmholtz resonator and a multidegree freedom (mdof) enclosure shows a very special feature. In fact, for a given resonator at one fixed location, no integral operation is involved in its discretized modal equation, which warrants an analytical solution by means of mathematical manipulation without any extra hypotheses. Therefore, the classical acoustic coupling problem between an enclosure and only one resonator is revisited using the present model. It differs from the previous work [1] in several aspects: (1) The present model considers a significant number of enclosure modes and uses point source to model the resonator radiation without suffering from the singularity problem; (2) it leads to a rigorous analytical solution for the sound pressure inside the enclosure as well as the volume velocity source strength out of the resonator aperture; (3) it provides a frequency equation to predict the frequency variation at the targeted mode as well as off-target ones shown in Part 3; (4) it presents a method to constrain the worsened noise level at off-target modes also shown in Part 3.

With only one resonator and N distributed point sources in the enclosure, the coupling equation is obtained from Eq. (9) after eliminating the subscribe m:

$$\left\{\frac{\omega^2-\left(\lambda_j^E\right)^2}{\omega^2}-A^R\frac{V^R\left[\varphi_j(\mathbf{r}^R)\right]^2}{V^E\quad\Lambda_j}\right\}\frac{P_j}{\dfrac{Q^S}{k^2V^E}}-\sum_{h\neq j}^{J}\left[A^R\frac{V^R}{V^E}\frac{\varphi_j(\mathbf{r}^R)\varphi_h(\mathbf{r}^R)}{\Lambda_j}\right]\frac{P_h}{\dfrac{Q^S}{k^2V^E}}=\sum_{n=1}^{N}\frac{\tilde{\varphi}_j(\mathbf{r}_n^S)}{\Lambda_j}\frac{Q_n^S}{Q^S}. \tag{14}$$

Note that if the targeted mode j is well separated with other modes, the summation term on the left-hand side of Eq. (14) can be ignored, leading to the approximate expression of modal response obtained by Fahy and Schofield [1]. In order to get an exact solution without this additional hypothesis, Eq. (14) is re-written as

$$\frac{\omega^2-\left(\gamma_j^E\right)^2}{\omega^2}\frac{P_j}{\dfrac{Q^S}{k^2V^E}}-A^R\frac{V^R}{V^E}\frac{\varphi_j(\mathbf{r}^R)}{\Lambda_j}\sum_{h=1}^{J}\varphi_h(\mathbf{r}^R)\frac{P_h}{\dfrac{Q^S}{k^2V^E}}=\sum_{n=1}^{N}\frac{\tilde{\varphi}_j(\mathbf{r}_n^S)}{\Lambda_j}\frac{Q_n^S}{Q^S}, \tag{15}$$

where $j = 1, 2, 3, \ldots$ When $\varphi_j(\mathbf{r}^R) \neq 0$, we divide $\varphi_j(\mathbf{r}^R)/\Lambda_j$ over the two sides of Eq. (15) and obtain

$$\frac{\omega^2 - \left(\gamma_j^E\right)^2}{\omega^2 \dfrac{\varphi_j(\mathbf{r}^R)}{\Lambda_j}} \frac{P_j}{\dfrac{Q^S}{k^2 V^E}} - A^R \frac{V^R}{V^E} \sum_{h=1}^{J} \varphi_h(\mathbf{r}^R) \frac{P_h}{\dfrac{Q^S}{k^2 V^E}} = \sum_{n=1}^{N} \frac{\tilde{\varphi}_j(\mathbf{r}_n^S)}{\varphi_j(\mathbf{r}^R)} \frac{Q_n^S}{Q^S}. \tag{16}$$

The physical meaning of $\varphi_j(\mathbf{r}^R) \neq 0$ is that the resonator is not located at any nodes of the enclosure modes. If $\varphi_j(\mathbf{r}^R) = 0$, Eq. (15) becomes

$$\frac{\omega^2 - \left(\gamma_j^E\right)^2}{\omega^2} \frac{P_j}{\dfrac{Q^S}{k^2 V^E}} = \sum_{n=1}^{N} \frac{\tilde{\varphi}_j(\mathbf{r}_n^S)}{\Lambda_j} \frac{Q_n^S}{Q^S}. \tag{17}$$

Eq. (17) shows that any resonator located at any nodes of the enclosure mode j provides no control actions to the mode.

Eq. (16) shows that the second term (summation term) on the left-hand side of the equation is a constant as the running modal index j varies. Applying the running indices to two arbitrary integers j and h, yields

$$\frac{\omega^2 - \left(\gamma_j^E\right)^2}{\omega^2 \dfrac{\varphi_j(\mathbf{r}^R)}{\Lambda_j}} \frac{P_j}{\dfrac{Q^S}{k^2 V^E}} - A^R \frac{V^R}{V^E} \sum_{i=1}^{J} \varphi_i(\mathbf{r}^R) \frac{P_i}{\dfrac{Q^S}{k^2 V^E}} = \sum_{n=1}^{N} \frac{\tilde{\varphi}_j(\mathbf{r}_n^S)}{\varphi_j(\mathbf{r}^R)} \frac{Q_n^S}{Q^S}, \tag{18}$$

$$\frac{\omega^2 - \left(\gamma_h^E\right)^2}{\omega^2 \dfrac{\varphi_h(\mathbf{r}^R)}{\Lambda_h}} \frac{P_h}{\dfrac{Q^S}{k^2 V^E}} - A^R \frac{V^R}{V^E} \sum_{i=1}^{J} \varphi_i(\mathbf{r}^R) \frac{P_i}{\dfrac{Q^S}{k^2 V^E}} = \sum_{n=1}^{N} \frac{\tilde{\varphi}_h(\mathbf{r}_n^S)}{\varphi_h(\mathbf{r}^R)} \frac{Q_n^S}{Q^S}. \tag{19}$$

The subtraction of Eqs. (19) and (18) allows the elimination of the constant terms, as follows:

$$\frac{\omega^2 - \left(\gamma_h^E\right)^2}{\omega^2 \dfrac{\varphi_h(\mathbf{r}^R)}{\Lambda_h}} \frac{P_h}{\dfrac{Q^S}{k^2 V^E}} - \frac{\omega^2 - \left(\gamma_j^E\right)^2}{\omega^2 \dfrac{\varphi_j(\mathbf{r}^R)}{\Lambda_j}} \frac{P_j}{\dfrac{Q^S}{k^2 V^E}} = \sum_{n=1}^{N} \left[\frac{\tilde{\varphi}_h(\mathbf{r}_n^S)}{\varphi_h(\mathbf{r}^R)} - \frac{\tilde{\varphi}_j(\mathbf{r}_n^S)}{\varphi_j(\mathbf{r}^R)} \right] \frac{Q_n^S}{Q^S}. \tag{20}$$

The above equation establishes a direct relationship between any two arbitrary enclosure modes, j and h. From Eq. (20), the modal response of P_h can be expressed in terms of P_j. Substituting P_h into Eq. (14), an analytical solution of P_j can be solved as

$$\frac{P_j}{\dfrac{Q^S}{k^2 V^E}} = \underbrace{\frac{\omega^2}{\omega^2 - \left(\gamma_j^E\right)^2} \sum_{n=1}^{N} \left[\frac{\tilde{\varphi}_j(\mathbf{r}_n^S)}{\Lambda_j} \frac{Q_n^S}{Q^S} \right]}_{\text{Contribution of the primary sound field}} + \underbrace{\frac{\left[\dfrac{\omega^2}{\omega^2 - \left(\gamma_j^E\right)^2} \dfrac{\varphi_j(\mathbf{r}^R)}{\Lambda_j} \right] A^R \dfrac{V^R}{V^E} \displaystyle\sum_{h=1}^{J} \left\{ \dfrac{\omega^2}{\omega^2 - \left(\gamma_h^E\right)^2} \dfrac{\varphi_h(\mathbf{r}^R)}{\Lambda_h} \displaystyle\sum_{n=1}^{N} \left[\tilde{\varphi}_h(\mathbf{r}_n^S) \dfrac{Q_n^S}{Q^S} \right] \right\}}{1 - A^R \dfrac{V^R}{V^E} \displaystyle\sum_{h=1}^{J} \left[\dfrac{\omega^2}{\omega^2 - \left(\gamma_h^E\right)^2} \dfrac{\varphi_h^2(\mathbf{r}^R)}{\Lambda_h} \right]}}_{\text{Contribution from the resonator}}. \tag{21a}$$

Using Eqs. (8), (21a), and $q^R(t) = S^R\dot{x}^R(t)\delta(\mathbf{r}-\mathbf{r}^R)$, the volume velocity source strength directed outward of the resonator into the enclosure can be found as

$$\frac{Q^R}{Q^S} = \frac{A^R\dfrac{V^R}{V^E}\displaystyle\sum_{h=1}^{J}\left\{\frac{\omega^2}{\omega^2-\left(\gamma_h^E\right)^2}\frac{\varphi_h(\mathbf{r}^R)}{\Lambda_h}\sum_{n=1}^{N}\left[\tilde{\varphi}_h(\mathbf{r}_n^S)\frac{Q_n^S}{Q^S}\right]\right\}}{1-A^R\dfrac{V^R}{V^E}\displaystyle\sum_{h=1}^{J}\left[\frac{\omega^2}{\omega^2-\left(\gamma_h^E\right)^2}\frac{\varphi_h^2(\mathbf{r}^R)}{\Lambda_h}\right]}. \tag{22}$$

From Eq. (22), it is known that the volume velocity source strength out of the resonator depends on its own acoustic parameters hidden in A^R, the source strength and the geometric dimensions of the primary sound source, the eigenvalues and mode shapes of the enclosure, and the volume ratio of the resonator and enclosure. It is also clear that when the resonator is put in the node of the jth enclosure mode, i.e., $\varphi_h(\mathbf{r}^R)=0$, the volume velocity induced by this mode is neutralized.

In terms of volume velocity source strengths, the modal pressure response shown in Eq. (21a) can be rewritten as

$$\frac{P_j}{\dfrac{Q^S}{k^2V^E}} = \underbrace{\frac{\omega^2}{\omega^2-\left(\gamma_j^E\right)^2}\sum_{n=1}^{N}\left[\frac{\tilde{\varphi}_j(\mathbf{r}_n^S)}{\Lambda_j}\frac{Q_n^S}{Q^S}\right]}_{\text{Contribution of the primary sound field}} + \underbrace{\frac{\omega^2}{\omega^2-\left(\gamma_j^E\right)^2}\frac{\varphi_j(\mathbf{r}^R)}{\Lambda_j}\frac{Q^R}{Q^S}}_{\text{Contribution from the resonator}} \tag{21b}$$

and the pressure $p(\mathbf{r})$ can be derived based on Eqs. (11) and (21b) as

$$\frac{p(\mathbf{r})}{\dfrac{\mathrm{i}\omega\rho_0Q^S}{V^Ek^2}} = \underbrace{-\sum_{h=1}^{J}\left\{\frac{\omega^2}{\omega^2-\left(\gamma_h^E\right)^2}\frac{\varphi_h(\mathbf{r})}{\Lambda_h}\sum_{n=1}^{N}\left[\tilde{\varphi}_h(\mathbf{r}_n^S)\frac{Q_n^S}{Q^S}\right]\right\}}_{\text{Contribution of the primary sound field}} \underbrace{-\frac{Q^R}{Q^S}\sum_{h=1}^{J}\left[\frac{\omega^2}{\omega^2-\left(\gamma_h^E\right)^2}\frac{\varphi_h(\mathbf{r})\varphi_h(\mathbf{r}^R)}{\Lambda_h}\right]}_{\text{Contribution from the resonator}}. \tag{23}$$

The above two analytical expressions for the modal response and for the pressure in the enclosure in terms of the volume velocity source strengths provide a more intuitionistic way to understand the result of the acoustic interaction inside the enclosure. They all include two parts: one induced by the primary sound field and the other contributed from the secondary sound field created due to the insertion of the resonator. Eq. (23) together with Eq. (22) also provide a useful analytical tool to optimally design the acoustic coupling system for desired noise attenuation inside the enclosure.

It should be stressed that the above mathematical manipulation only applies to the case of one single resonator coupled with an enclosure. When two or more resonators are present, Eq. (9) describing the fully coupled linear system should be solved using a numerical inversion method. It has been proved that the analytical result obtained from Eq. (23) is identical as the numerical one calculated from a fully coupled model using the matrix inversion. It is also noticed that, during the above derivation, because the modal response is solved before calculating the sound pressure inside the enclosure and the volume velocity of the resonator, the present model does not suffer from the singularity problem as encountered in Ref. [4].

In order to compare the results obtained in this study with those presented in Refs. [1,4], a sound pressure level (SPL) presented in Ref. [4] is used to determine the pressure distribution inside the enclosure

$$L_p(\mathbf{r}) = 20\log\left|\frac{p(\mathbf{r})}{\dfrac{\mathrm{i}\omega\rho_0Q^S}{V^Ek^2}}\right|. \tag{24}$$

3. Simulations

Numerical simulations were designed to examine the present model and to compare with the past experimental and theoretical results. In the calculations, a series of classical Helmholtz resonators and one right parallepiped reverberant enclosure were used. The directions along width, height, and length were

defined as x-, y- and z-direction, respectively. The geometric dimensions of the enclosure were $l_x = 2.1$ m, $l_y = 2.52$ m, and $l_z = 2.5$ m, which were also used by Fahy and Schofield [1] and Cummings [4]. Helmholtz resonators, having a 306 mm internal diameter cylindrical body with a variable depth and a 102 mm internal diameter neck with a 150 mm physical neck length, were inserted in the enclosure at places not too near the node of the enclosure mode under consideration [1,4]. In Ref. [1], one or two sheets of loudspeaker grill cloth were introduced to the base of the neck to improve the resonator's internal resistance. One square source (loudspeaker) with dimensions of 158 mm in the x and y directions and zero in z direction was installed at (79, 79, 10) mm to drive the primary sound field [4]. One Brüel and Kjær Type $4135^{1/4}$'' microphone located at (1.94, 0.16, 0.16) m was used to measure SPL inside the enclosure [1]. Relevant information about the geometry and positions associated with the enclosure, resonators, and measurement devices is tabulated in Table 1.

Table 1
Geometric dimensions and location information

Device	Parameter	Data
Enclosure	Dimensions (m)	
	l_{ex}	2.10
	l_{ey}	2.52
	l_{ez}	2.50
	Neck radius, r_1 (mm)	51
	Neck length, l_1 (mm)	105
	Body radius, r_2 (mm)	153
	Body length, l_2 (mm)	100.1
Resonators	Internal resistance, R_i (mks Rayls)	
	Empty necked	2.7
	One sheet of cloth	12.6
	Two sheets of cloth	20.8
Loudspeaker	Dimensions (mm)	
	l_{sx}	158
	l_{sy}	158
	l_{sz}	0
	Location, (x_s, y_s, z_s) (mm)	(79, 79, 10)
Microphone	Location, (x_m, y_m, z_m) (m)	(1.94, 0.16, 0.16)

Table 2
Computed natural frequencies and measured Q-factors for enclosure modes

Index	Mode number (l m n)	Natural frequency (Hz)	Q-factor
1	000	0	56
2	010	69.6	56
3	001	70.2	56
4	100	83.6	56
5	011	98.9	56
6	110	108.8	56
7	101	109.1	56
8	111	129.5	35
9	020	139.3	32
10	002	140.4	32
11	021	156.0	41
12	012	156.7	41
13	120	162.4	46
—	—	>160.0	46

Table 3
Physical parameters

Physical parameter	Used value
Ambient temperature, T (°C)	33
Speed of sound, c (m/s)	351
Density of air, ρ_0 (kg/m^3)	1.2
Specific heat ratio of air, γ	1.402
Thermal conductivity of air, κ (W/m K)	0.0263
Specific heat at constant pressure of the air, Cp (J/kg K)	1.01×10^3
Coefficient of shear viscosity, μ (Pa s)	1.85×10^{-5}

The thermal-viscous boundary conditions were considered for the enclosure, and the eigenfunctions of the enclosure $\varphi_j(\mathbf{r}^R)$ corresponding to the eigenvalues $\gamma_j^E = \omega_j^E + \mathrm{i}C_j^E$ were well presented in Ref. [4], where ω_j^E was the natural frequency of the jth enclosure mode in the absence of damping and C_j^E was the jth *ad hoc* damping coefficient obtained from measured Q-factors using $C_j^E = \omega_j^E/2Q_j^E$. A total of 216 enclosure modes [$(l,m,n) = (0\sim5,0\sim5,0\sim5)$, where l, m, n are the node number in x-, y-, and z-direction, respectively] were considered in the calculation. The Q-factors of the enclosure modes were shown in Table 2, which were measured by Fahy and Schofield [1] and also used by Cummings [4]. The ambient temperature inside the enclosure was 33 °C and the sound speed at this temperature was $c = 351$ m/s [4]. All physical parameters used in computation are listed in Table 3.

3.1. Comparison between experiment and theory

In the configuration used for comparisons, a resonator was put in the right parallelepiped enclosure at (1.94, 2.0, 0.16) m. Experimental data reported by Fahy and Schofield [1] were used as benchmark results. In that work, three unflanged resonators (empty necked, with one or two sheet of cloth) were designed and tuned under anechoic conditions to target the enclosure mode (1 1 1) at 129.5 Hz. The Q-factors of the three resonators were experimentally determined in Ref. [1], giving $Q_R = 75$, 16, and 9.7, respectively. It is known that the internal resistance of the resonator can be estimated by $R_i = \omega^R \rho_0 L^R/Q_R$ [1]. It therefore depends on the resonance frequency, the Q-factor, and the effective neck length of the resonator. The effective neck length used by Fahy and Schofield [1] only considers the exterior end correction, giving $R_i = 2.4$, 11.1, and 18.2 mks Rayls. When considering both the exterior and interior end corrections in the calculation of the effective neck length, the internal resistance becomes $R_i = 2.7$, 12.6, and 20.8 mks Rayls, which were used in this study. Note that Cummings [4] used 2.98 and 14 mks Rayls for a resonator with an empty neck and with one sheet of cloth in the neck, respectively.

The SPL at the microphone position was measured by Fahy and Schofield [1] as the excitation frequency of loudspeaker was varied. The measured SPL curves are shown in Fig. 1(a), in which the solid-line, dashed-line, and dotted-line correspond to the measured SPL without resonator, with an empty-necked resonator $R_i = 2.7$ mks Rayls, and with a damped resonator $R_i = 12.6$ mks Rayls, respectively. Each peak of the measured SPL curve without resonator is associated with one enclosure mode. After the empty-necked resonator is inserted, the peak at 129.5 Hz is split to two (127.0 and 133.0 Hz) unequally located on each side of the original resonance frequency (129.5 Hz) due to a strong coupling between the lightly damped resonator ($R_i = 2.7$ mks Rayls) and the targeted enclosure mode (1 1 1). The separation between the two coupled frequencies is determined by the volume ratio of the resonator to the enclosure [1]. When increasing the damping of the resonator from $R_i = 2.7$ to 12.6 mks Rayls, the two peaks are damped with a smooth amplitude variation.

Based on the same configurations, calculations using the present model and Cummings's model were carried out, resulting in two sets of figures: Figs. 1(b) and (c), respectively. In comparison with Fig. (1a), it can be observed that, around the targeted region, the overall shape of the predicted SPL curve using the present

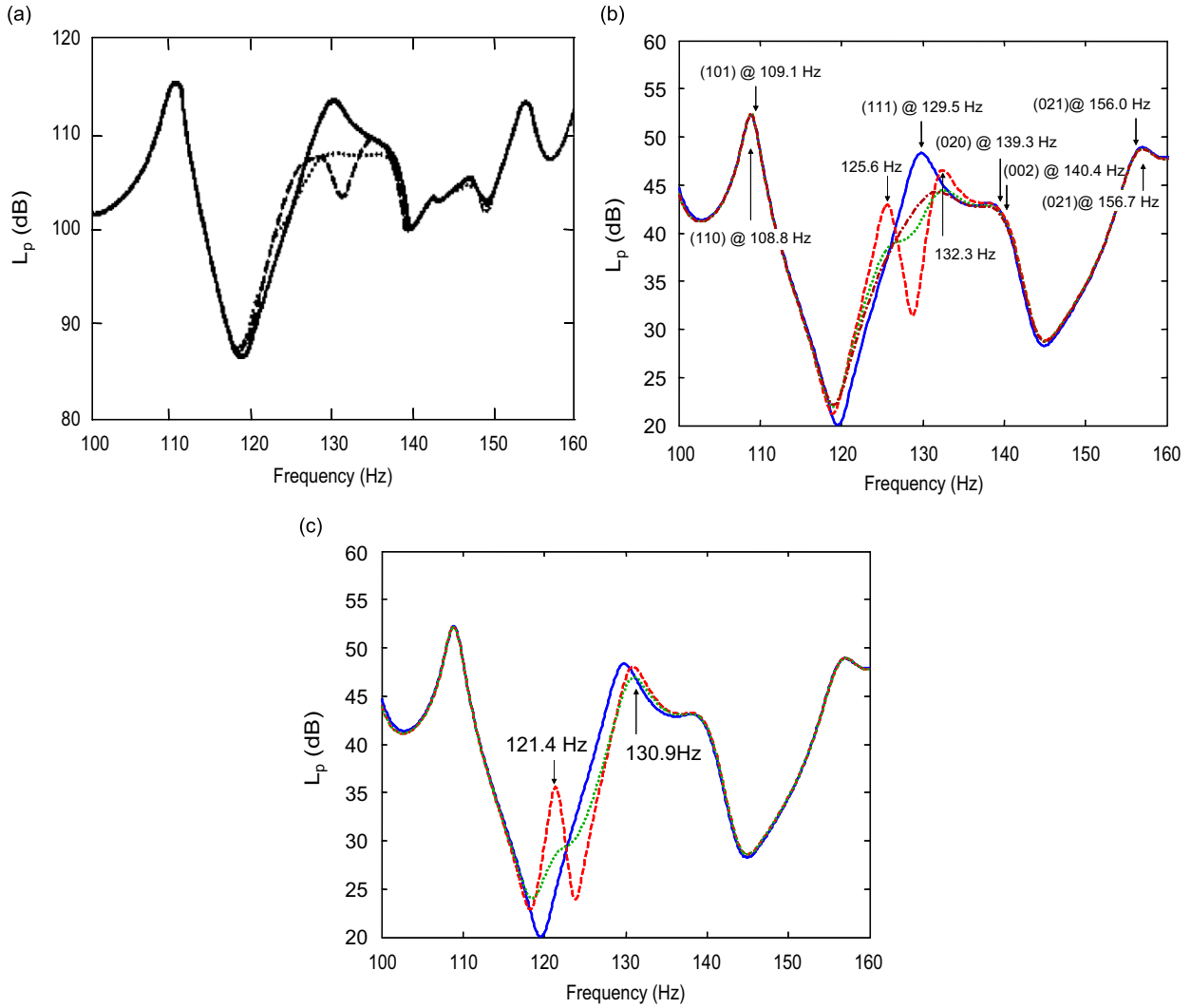

Fig. 1. SPL curves at (1.94, 0.16, 0.16) m: (a) Fahy and Schofield's measurements: —, without resonator; — —, with an empty-necked resonator, $r = 2.7$ mks Rayls; · · · ·, with a damped resonator, $r = 12.6$ mks Rayls. (b) Present model: —, without resonator; — —, with an empty-necked resonator, $r = 2.7$ mks Rayls; · · · ·, with a damped resonator, $r = 12.6$ mks Rayls, — · —, with a damped resonator, $r = 20.8$ mks Rayls. (c) Cummings's model: —, without resonator; — —, with an empty-necked resonator, $r = 2.7$ mks Rayls; · · · ·, with a damped resonator, $r = 12.6$ mks Rayls.

model (Fig. (1b)) is quite similar to that of the measured data (Fig. (1a)), although the predicted dip near 129.5 Hz with an empty-necked resonator is deeper than the measured one and the predicted SPL data between the two coupled frequencies are also slightly lower than the measured values. From Fig. (1b), it can be also noticed that an increase in the internal damping of the resonator does not always warrant a systematic improvement of the control at the targeted frequency, e.g. at 129.5 Hz. When internal resistance increases from 2.7 to 12.6 mks Rayls, the control performance of the resonator is significantly improved. However, if the resistance further increases to 20.8 mks Rayls, the control performance deteriorates at 129.5 Hz when compared with 12.6 Rayls case. This observation suggests that the damping of the resonator cannot be excessively large because the energy dissipation mechanism of the resonator depends on both damping and vibrating velocity. Actually, $R_i = 12.6$ mks Rayls was experimentally determined as a "near optimum" damping by Fahy and Schofield [1].

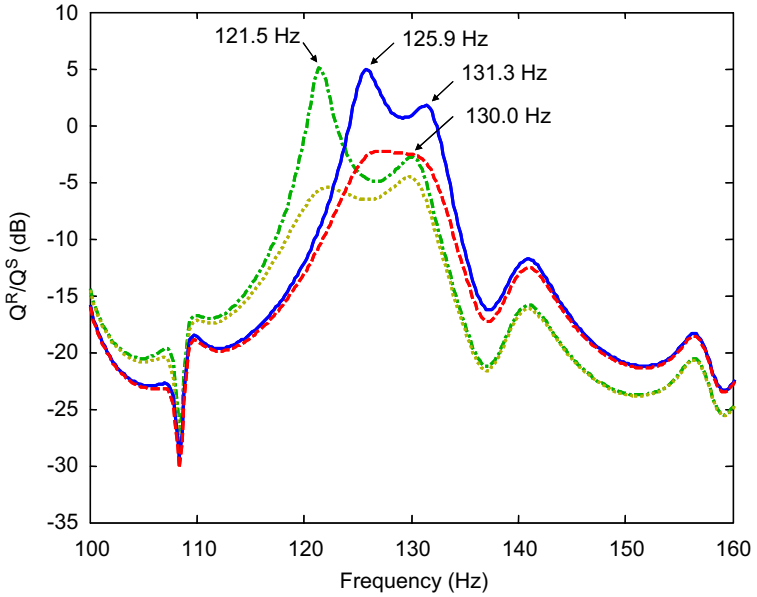

Fig. 2. Volume velocity source strength out of the Helmholtz resonator: Present model: —, with an empty-necked resonator, $r = 2.7$ mks Rayls; — —, with a damped resonator, $r = 12.6$ mks Rayls; Cummings's model: — · — with an empty-necked resonator, $r = 2.7$ mks Rayls; · · · ·, with a damped resonator, $r = 12.6$ mks Rayls.

When comparing Figs. 1(b) and (c), a significant discrepancy is observed between the present model and Cummings's model. A plausible reason is that when Cummings calculated pressure at the resonator aperture, an equivalent small pulsating sphere was used to approximate the resonator radiation in order to avoid the singularity induced by directly using the volume velocity out of the resonator. Such an approximation results in a relatively large error in terms of the coupled frequencies: 121.4 and 130.9 Hz as predicted by Cummings's model vs. 127.0 and 133.0 Hz as measured by Fahy and Schofield [1] (the coupled frequencies are 125.6 and 132.3 Hz predicted by the present model). This error impacts on the accuracy of the prediction at the targeted mode at 129.5 Hz.

The volume velocity source strength out of the resonator computed from the analytical solution shown in Eq. (22) was compared with that obtained from Cummings's model (Fig. 2). When the resonator was lightly damped, two coupled frequencies can be clearly identified in the curves. Obviously, the difference in terms of coupled frequencies between the two models leads to different profiles of the secondary source in frequency domain, such resulting in different acoustic coupling between the resonator and enclosure and different response in the enclosure (see Figs. 1(b) and (c)). From Fig. 2, it is also found that as the damping of the resonator increases, the peak of the volume velocity source strength is smoothed into a plateau with a reduced magnitude. It can be concluded that the secondary sound field produced by the resonator behaves like a narrowband speaker, whose bandwidth depends on the coupled frequencies, and whose strength is associated with the internal resistance of the resonator and the primary sound source strength. Notice that the two coupled frequencies (125.9 and 131.3 Hz) obtained from the volume velocity sound strength curve computed by present model are slightly different with those identified from the SPL curve (125.6 and 132.3 Hz), which is caused with the term $i\omega/((\omega^R)^2 - \omega^2 + icR\omega$ shown in Eq. (8).

It is pertinent to mention that during the calculations using both models, the effects of the number of enclosure modes being taken into account were also investigated. When the number of the enclosure modes was varied from 216 ($l = m = n = 0\sim5$) to 1000 ($l = m = n = 0\sim9$), the volume velocity of the resonator and the SPL in the enclosure predicted with Cummings's model and present model underwent no changes (not shown). It implied that (1) 216 enclosure modes were sufficient to ensure the convergence of the solution, and (2) the scattering of an equivalent pulsating sphere used in Cummings's model did not converge to the

radiation of a point source even thought the number of the enclosure modes used in computation was considerably large.

3.2. Coupled and shifted frequencies

The above simulations have shown the importance of the coupled frequencies in the acoustic interaction between the enclosure and resonator and in the prediction of the performance of resonators. Therefore, using the established model, the variation of the enclosure resonance frequencies after inserting one resonator into the enclosure is investigated hereafter.

In the absence of the primary sound field in the enclosure, Eq. (15) describes the free vibration behavior of the coupled system as follows:

$$\left[\omega^2-\left(\gamma_j^E\right)^2\right]P_j-\omega^2A^R\frac{V^R}{V^E}\frac{\varphi_j(\mathbf{r}^R)}{\Lambda_j}\sum_{h=1}^{J}\varphi_h(\mathbf{r}^R)P_h=0. \tag{25}$$

This leads to a frequency equation expressed as

$$\frac{\left(\omega^R\right)^2}{\omega^2-\mathrm{i}cR\omega-\left(\omega^R\right)^2}\sum_{h=1}^{J}\left[\varepsilon_h^2\frac{\omega^2}{\omega^2-\left(\gamma_h^E\right)^2}\right]-1=0, \tag{26}$$

where $\varepsilon_h^2=\varphi_h^2(\mathbf{r}^R)V^R/\Lambda_hV^E$; ε_h is a coupling parameter between the hth enclosure mode and the resonator [1]. From Eqs. (15) or (25), it is found that, after inserting a resonator into the enclosure, the resonator is coupled with all acoustic modes of the enclosure. If a significant coupling occurs at only the targeted mode h_j while neglecting all others, two coupled frequencies can be obtained, which are approximately equally located at either side of the original frequency with $\Delta\omega=\varepsilon_{h_j}\omega^R$ [1]. Unfortunately, most enclosure modes are not well separated in frequency due to a relatively high modal-density of the enclosure. Thus, when a resonator is put to the enclosure near the anti-node of the targeted mode, significant acoustic coupling occurs not only at the targeted mode but also occurs at other modes bordering upon the targeted mode. Assuming that the acoustic coupling occurring at H enclosure modes $h=\{h_1,h_2,\ldots,h_j,\ldots,h_H\}$, including the targeted mode h_j, is significant, after ignoring the damping effects in both the enclosure and resonator, the frequency Eq. (26) becomes

$$\left[\left(\omega^R\right)^2-\omega^2\right]^2\prod_{\mathrm{i}\in\mathbf{h},\mathrm{i}\neq h_j}\left[\omega^2-\left(\omega_i^E\right)^2\right]-\left(\omega^R\right)^2\sum_{i\in\mathbf{h}}\left\{\varepsilon_{\mathrm{i}}^2\omega^2\prod_{m\in\mathbf{h},m\neq i}\left[\omega^2-\left(\omega_m^E\right)^2\right]\right\}=0. \tag{27}$$

Mathematically speaking, there exist $(H+1)$ positive real frequencies satisfying Eq. (27) for a practical coupling system: two coupled frequencies and other $(H-1)$ new frequencies different from the original off-target resonance frequencies, which can be characterized by a frequency shift after inserting the resonator. For an example, in order to better examine this phenomenon, the above problem is simplified to keep only two coupled enclosure modes A at ω^R and B at ω_B^E, in which mode A is the targeted mode by the resonator. In such case, Eq. (27) becomes

$$\left[\left(\omega^R\right)^2-\omega^2\right]^2\left[\omega^2-\left(\omega_B^E\right)^2\right]-\varepsilon_A^2\left(\omega^R\right)^2\omega^2\left[\omega^2-\left(\omega_B^E\right)^2\right]-\varepsilon_B^2\left(\omega^R\right)^2\omega^2\left[\omega^2-\left(\omega^R\right)^2\right]=0.$$

It can be proved that (1) three positive real frequencies can be obtained from above equation, (2) acoustic coupling gives rise to new resonances: for the targeted mode A, two coupled frequencies occurring at each side of the targeted resonance frequency to replace the original frequency (ω^R); for the off-target mode B, acoustic coupling results in a frequency shift to create a new frequency to replace the off-target resonance frequency (ω_B^E), and (3) both the coupled and shifted frequencies depend on the coupling parameters ε_h.

In the following simulation, one empty-necked Helmholtz resonator for controlling the enclosure mode (0 1 0) at 69.6 Hz was designed and put at (0.2, 0.16, 0.2) m inside the enclosure to demonstrate the coupled frequencies at the targeted frequency and shifted frequency at other off-target modes. The Q-factor of the resonator was assumed to be $Q_r=75$. The computed SPLs at the microphone position (1.94, 0.16, 0.16) m without resonator and with the empty-necked resonator are shown in Fig. 3. The natural frequencies of the

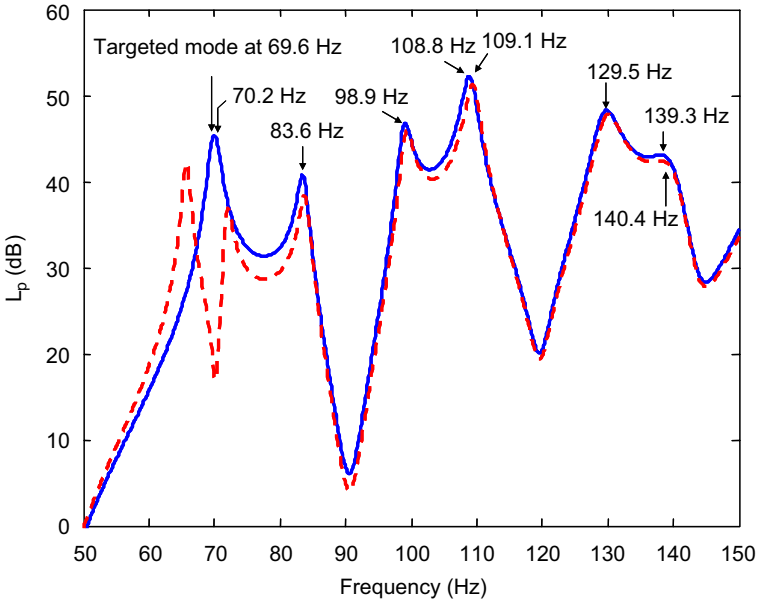

Fig. 3. Predicted SPL curves at (1.94, 0.16, 0.16) m: — , without resonator; · · · · , with a 69.6 Hz empty-necked Helmholtz resonator at (0.2, 0.16, 0.2) m.

Table 4
Coupled and shifted frequencies of an enclosure with a resonator inserted at (0.2, 0.16, 0.2) m

Natural frequencies with no resonator (Hz)	Natural frequencies with one resonator at (Hz)	Frequency shift (Hz)
69.6	66.3	Coupled
Targeted	69.9	Frequencies
70.2	72.3	2.1
83.6	83.9	0.3
98.9	99.2	0.3
108.8	108.9	0.1
109.1	109.5	0.4
129.5	129.8	0.3
139.3	139.4	0.1
140.4	140.5	0.1

enclosure are also marked in the figure to visualize the frequency change before and after the insertion of the resonator. It can be observed that, after introducing the 69.6 Hz Helmholtz resonator into the enclosure, two peaks at 65.7 and 72.1 Hz are generated to replace the original peak at 70.1 Hz and other off-target natural frequencies have obvious shift when comparing with their counterparts without resonator. The predicted coupled and shifted frequencies using Eq. (27) when all ten modes in 0∼150 Hz were taken into account in the coupling are listed in Table 4. The maximum frequency shift of 2.1 Hz occurs at mode (0 0 1) at 70.2 Hz because this mode is near the targeted mode (0 1 0) in frequency, and frequency shift at other off-target modes is no larger than 0.4 Hz.

3.3. Constraint on the worsened SPL at off-target resonances

At some off-target resonances, the frequency shift at off-target modes may be accompanied by a worsened SPL. Two methods can be used to vary the acoustic coupling to constrain or improve this deterioration: (1) relocating resonators in the enclosure, and (2) changing the number of the resonator in an array. It is

evident that locations of the resonators impact on the way they are coupled to the enclosure. As an extreme case, when putting a resonator close to the node of an off-target enclosure mode M, the zero value of $\varphi_M(\mathbf{r}^R)$ disables the acoustic coupling between the resonator and this enclosure mode, causing no effect on it. In a more likely scenario where $\varphi_M(\mathbf{r}^R)\neq 0$ (off-target mode M), assuming that the frequency shift is very small after inserting a resonator, and only mode M dominates the response of the enclosure at its resonance frequency ω_M, the insertion of the resonator may not reduce or even amplify the SPL at ω_M inside the enclosure, which can be expressed as $|P_1(\omega_M)| \geqslant |P_0(\omega_M)|$, where P_0 and P_1 represent the Mth modal response of the enclosure at ω_M without and with a resonator, respectively. From Eqs. (21a) and (12) we have

$$P_1(\omega_M) - P_0(\omega_M) = \frac{A^R \dfrac{V^R}{V^E} \dfrac{\omega_M^2}{\omega_M^2 - \left(\gamma_M^E\right)^2} \dfrac{\varphi_M(\mathbf{r}^R)}{\Lambda_M} \displaystyle\sum_{h=1}^{J} \left\{ \dfrac{\omega_M^2}{\omega_M^2 - \left(\gamma_h^E\right)^2} \dfrac{\varphi_h(\mathbf{r}^R)}{\Lambda_h} \displaystyle\sum_{n=1}^{N} \left[\dfrac{Q_n^S}{Q^S} \tilde{\varphi}_h(\mathbf{r}_n^S) \right] \right\}}{1 - A^R \dfrac{V^R}{V^E} \displaystyle\sum_{h=1}^{J} \left[\dfrac{\omega_M^2}{\omega_M^2 - \left(\gamma_h^E\right)^2} \dfrac{\varphi_h^2(\mathbf{r}^R)}{\Lambda_h} \right]}. \tag{28}$$

Based on a triangle inequality $||A| - |B|| \leqslant |A - B|$, if $|A| \geqslant |B|$ and if we can find a position for the resonator so that $|A-B| = 0$, we will have $|A| = |B|$. This implies that through adjusting the resonator location inside the enclosure in such a way that $|P_1(\omega_M) - P_0(\omega_M)| = 0$, we have $|P_1(\omega_M)| = |P_0(\omega_M)|$ which leads to

$$\left| \sum_{h=1}^{J} \left\{ \frac{\omega_M^2}{\omega_M^2 - \left(\gamma_h^E\right)^2} \frac{\varphi_h(\mathbf{r}^R)}{\Lambda_h} \sum_{n=1}^{N} \left[\frac{Q_n^S}{Q^S} \tilde{\varphi}_h(\mathbf{r}_n^S) \right] \right\} \right| = 0. \tag{29}$$

Eq. (29) ensures that after inserting a resonator into the enclosure, the SPL at the off-target mode M can be constrained at the value before the resonator is installed. We use the left-hand side term over the Mth modal response $P_0(\omega)$ to define a new variable as follows:

$$\sigma(\omega, \mathbf{r}^R) = \left| \frac{\displaystyle\sum_{h=1}^{J} \left\{ \frac{\omega^2}{\omega^2 - \left(\gamma_h^E\right)^2} \frac{\varphi_h(\mathbf{r}^R)}{\Lambda_h} \sum_{n=1}^{N} \left[\tilde{\varphi}_h(\mathbf{r}_n^S) \frac{Q_n^S}{Q^S} \right] \right\}}{\dfrac{\omega^2}{\omega^2 - \left(\gamma_M^E\right)^2} \displaystyle\sum_{n=1}^{N} \left[\frac{\tilde{\varphi}_M(\mathbf{r}_n^S)}{\Lambda_M} \frac{Q_n^S}{Q^S} \right]} \right|. \tag{30}$$

Through adjusting $\mathbf{r}^R$ inside the enclosure to minimize the value of $\sigma(\omega_M, \mathbf{r}^R)$, the worsened SPL can be minimized. It should be noted that an improvement at a specific mode at a specific location does not

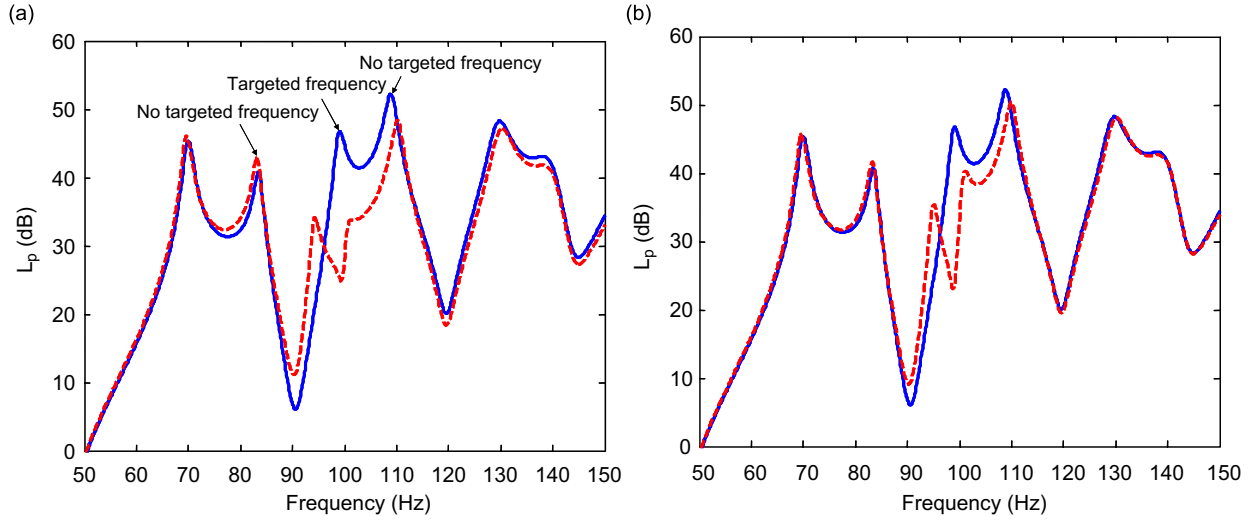

Fig. 4. Predicted SPL curves at (1.94, 0.16, 0.16) m: — in (a) and (b), without resonator; — — in (a), with a 98.9 Hz Helmholtz resonator at (0.16, 0.16, 0.16) m; — — in (b), with a 98.9 Hz resonator at (0.4, 0.2, 0.15) m.

necessarily mean an overall improvement. Otherwise, a spatially and temporally averaged SPL must be considered [4].

A numerical test was conducted using Eq. (30) to determine the position for the resonator to minimize the worsened SPL at 83.6 Hz after inserting a 98.9 Hz Helmholtz resonator at (0.16, 0.16, 0.16) m in the enclosure. The 98.9 Hz resonator with $Q_r = 75$ was designed to target the enclosure mode (0 1 1). The predicted SPL curves without and with the resonator are shown in Fig. (4a). It can be seen that, after inserting the resonator, the SPLs at around 98.9 Hz (targeted frequency), 108.8 and 109.1 Hz (off-target frequencies) are significantly

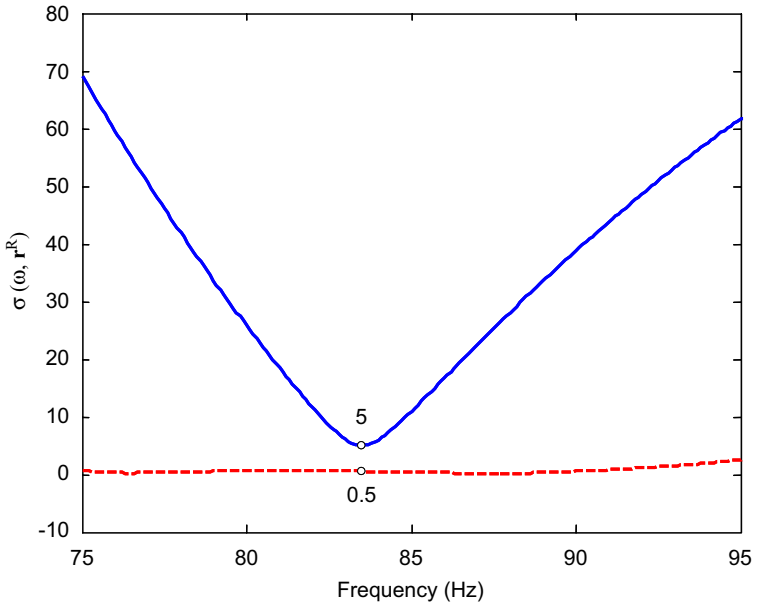

Fig. 5. Computed $\sigma(\omega, \mathbf{r}^R)$. —, resonator located at $\mathbf{r}^R = (0.16, 0.16, 0.16)$ m; — —, resonator located at $\mathbf{r}^R = (0.4, 0.2, 0.15)$ m.

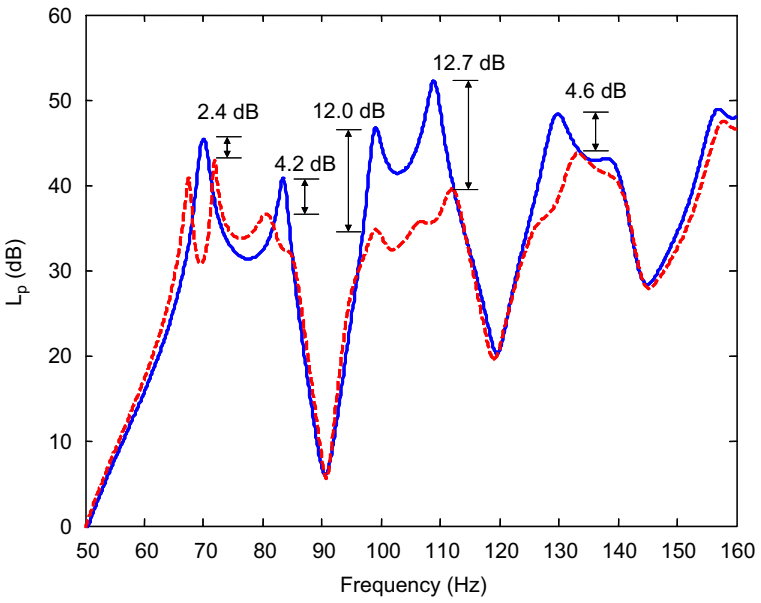

Fig. 6. Predicted SPL curves at (1.94, 0.16, 0.16) m: —, without resonator; — — with a resonator array, including five resonators.

attenuated. However, the SPL at 83.6 Hz (off-target frequency) is increased by 2 dB. Location optimization using Eq. (30) yields a new location at (0.4, 0.2, 0.15) m for resonator installation, with SPL results shown in Fig. (4b). It can be seen that, after installing the resonator, the SPL at 83.6 Hz is maintained along with acceptable reduction at other major frequencies. Curves showing the variation of $\sigma(\omega, \mathbf{r}^R)$ before and after changing the resonator location are plotted in Fig. 5. It can be seen that the optimization process reduces σ from 5 to 0.5 at 83.6 Hz.

Although the change of location proposed in the above optimization process can minimize the deteriorated SPL at an off-targeted mode, this effort is accompanied by a degraded control performance at 98.9, 108.8 and 109.1 Hz shown in Fig. 4. As an alternative, by using a resonator array consisting of several different resonators, the acoustic coupling between the enclosure and resonators can be adjusted to further improve the sound reduction in a large frequency band. This method can also overcome the inherent narrowband property of a single Helmholtz resonator and provide significant control over a relatively broad frequency band. The general model, which was shown as a set of linear equations Eq. (9), was applied to show this possibility. As an example, a resonator array consisting of five Helmholtz resonators located at (0.5, 0.16, 0.2) m, (0.16, 0.5, 0.5) m, (0.16, 0.16, 0.16) m, (1.7, 0.16, 0.16) m, and (1.94, 2.0, 0.16) m was designed to target the enclosure mode (0 1 0) at 69.6 Hz, (1 0 0) at 83.6 Hz, (0 1 1) at 98.9, (1 1 0) at 108.8, and (1 1 1) at 129.5 Hz, respectively. All resonators were damped by one piece of material in their necks, and the Q-factor of the resonators at their resonance frequencies was assumed as $Q_r = 16$. Again, 216 enclosure modes were considered in the simulations. The predicted SPLs at (1.94, 0.16, 0.16) m in the frequency band of [50,160] Hz were shown in Fig. 6. It can be seen that obvious sound reduction was achieved at all targeted modes, with reduction levels ranging from 2.4 to 12.7 dB.

4. Conclusions

This paper presents a general model to deal with the acoustic coupling between an enclosure and an acoustic resonator array, which leads to a simplified model when the array retreats to one resonator. Analytical solutions for sound pressure in the enclosure and volume velocity out of the resonator aperture were derived in the case of an enclosure coupled with only one resonator. This allowed us to reexamine some of the previous studies reported in the literature. Data obtained from the present model showed a remarkable agreement with those measured by Fahy and Schofield and an obvious difference with those computed from Cummings's theory. An optimal equation for determining the location of a resonator to constrain the worsened SPL at an off-target resonance was provided. Computed volume velocity source strength out of the resonator aperture showed that the resonator behaves like a narrowband speaker, with its bandwidth depending on the coupled frequencies of the enclosure and the resonator, and its strength associated with the primary sound source strength and the internal resistance of the resonator. It was shown that the insertion of a lightly damped resonator splits the targeted resonance frequency into two new coupled frequencies, together with a shift of other off-target resonance frequencies. These frequency variations can be accurately predicted using the present model. It was also shown that the position of resonators significantly affects the acoustic coupling, and therefore the noise control performance. The presented model can be used to determine the optimal location of the resonator to constrain the SPL at an off-target resonance on the one hand, and to optimally design a resonator array to achieve a better control over a relatively broad frequency band on the other hand. The proposed model provides a useful tool for the design of an acoustic resonator array in interior noise control applications, which currently still involves heavy experimental measurements on a trial-and-error basis.

Acknowledgments

The authors wish to acknowledge a grant from Research Grants Council of Hong Kong Special Administrative Region, China (Project No. PolyU 5137/06E) and support by the Central Research Grant of The Hong Kong Polytechnic University through grant G-YE67.

References

[1] F.J. Fahy, C. Schofield, A note on the interaction between a Helmholhtz resonator and an acoustic mode of an enclosure, *Journal of Sound and Vibration* 72 (1980) 365–378.
[2] F.J. Van Leeuwen, The damping of eigen-tones in small rooms by Helmholtz resonators, European Broadcasting Unio Review, A—Technical, Vol. 62, 1960, pp. 155–161.
[3] H.R. Britz, H.F. Pollard, Computational analysis of coupled resonators, *Journal of Sound and Vibration* 60 (1978) 305–307.
[4] A. Cummings, The effects of a resonator array on the sound field in a cavity, *Journal of Sound and Vibration* 154 (1992) 25–44.
[5] D.T. Blackstock, *Fundamentals of Physical Acoustics*, Wiley, New York, 2000.
[6] K.U. Ingard, On the theory and design of acoustic resonators, *Journal of the Acoustical Society of America* 25 (1953) 1037–1061.
[7] A.D. Pierce, *Acoustics: An Introduction to its Physical Principles and Applications*, The Acoustical Society of America, 1989.
[8] K.P. Flynn, R.L. Panton, The interaction of Helmholtz resonators in a row when excited by a turbulent boundary layer, *Journal of the Acoustical Society of America* 87 (1990) 1482–1488.
[9] C.Q. Howard, B.S. Cazzolato, C.H. Hansen, Exhaust stack silencer design using finite element analysis, *Noise Control Engineering Journal* 48 (2000) 113–120.
[10] D. Li, J.S. Vipperman, Noise control of a ChamberCore payload fairing using integrated acoustic resonators, *Journal of Spacecraft and Rockets* 43 (2006) 877–882.
[11] E.H. Dowell, G.F. Gorman, D.A. Smith, Acoustoelasticity: general theory, acoustic natural modes and forced response to sinusoidal excitation, including comparisons with experiment, *Journal of Sound and Vibration* 52 (1977) 519–542.
[12] F.J. Fahy, *Sound and Structural Vibration: Radiation, Transmission and Response*, Academic Press, London, 1993.